Versão do arquivo anexado / Version of attached file:

Versão do Editor / Published Version

Mais informações no site da editora / Further information on publisher's website:

https://www.sciencedirect.com/science/article/pii/S092583881832440X

DOI: 10.1016/j.jallcom.2018.06.319

Direitos autorais / Publisher's copyright statement:

Heat treatments effects on functionalization and corrosion behavior of Ti-6Al-4V ELI alloy made by additive manufacturing

Guilherme Arthur Longhitano [a, b, *], Maria Angeles Arenas [c], Ana Conde [c],
Maria Aparecida Larosa [a, d], André Luiz Jardini [a, d], Cecília Amélia de Carvalho Zavaglia [a, b],
Juan José Damborenea [c]

[a] National Institute of Biofabrication (INCT-BIOFABRIS), Albert Einstein Avenue 500, Campinas, Brazil
[b] School of Mechanical Engineering, State University of Campinas, Mendeleyev Street 200, Campinas, Brazil
[c] National Center for Metallurgical Research (CENIM-CSIC), Gregorio del Amo Avenue 8, Madrid, Spain
[d] School of Chemical Engineering, State University of Campinas, Albert Einstein Avenue 500, Campinas, Brazil

ABSTRACT

Additive manufacturing has emerged in recent years as one of the most in-demand technology for manufacturing of prototypes and components with complex geometries. Its application in biomedicine shows a big productive potential concerning customized implants with optimized geometries, reducing risks of rejection and achieving better ergonomic results. However, Ti-6Al-4V ELI pieces produced by Direct Metal Laser Sintering (DMLS) need a post heat treatment in order to reach optimum mechanical properties as well as to release internal stresses resulted from the manufacturing process. This study aims at analyzing the change of microstructure in DMLS samples by effect of heat treatments and its influence in the corrosion behavior and in the anodizing process. The surfaces were analyzed by 3D confocal profilometry, scanning electron microscopy and energy dispersive X-ray spectroscopy. DMLS samples showed different microstructures after heat treatments in the range from 650 to 1050 °C. The main difference in the microstructures is the nucleation and growth of β phase, which could have a detrimental effect on its corrosion behavior. The corrosion behavior was studied by cyclic potentiodynamic polarization in phosphate buffered saline solution at 37 °C. After anodizing, an oxide film was grown on the material surface, composed of a barrier and a nanoporous layer doped with F ions. The passive current density was reduced by approximately two orders of magnitude for all conditions, despite morphological differences on the layers. This is not only an improvement of the corrosion resistance but also a decrease in the ion release into bloodstream.

© 2018 Elsevier B.V. All rights reserved.

1. Introduction

Metallic materials are the most widely used ones for load-bearing implants due to several advantages in relation to other materials: high strength and resistance to fracture, ease of fabrication of both simple and complex shapes, corrosion resistance and biocompatibility [1]. However, metallic materials are prone to corrosion when working in aggressive environment. Living tissues are a complex system composed of cells and biomolecules (organic and inorganic) that contains different chemical elements, including a relatively high chloride concentration. Therefore, the implant surface will have to interact with these tissues with the challenge of achieving adsorption of cells and proteins providing an excellent surface for organisms to attach to and remain for the entire duration of the implant [2,3]. Although joint replacement surgery has become an extremely successful operation (>90% after 10 years and ≈85% after 20 years). As life expectancy is increasing, the number of orthopedic surgeries, especially partial or total joint replacement, will also grow in the next years. This will make for an enormous challenge for biomaterials that will have to withstand over a long period of time. The development of new materials and manufacturing processes are crucial tools for increasing the service life and performance of implants [3,4].

Additive manufacturing (AM) is a technique recently used as tool in medicine for manufacturing of customized implants and biomodels [5]. AM presents capacity of building highly complex geometries directly from a CAD model, which permits fabrication of custom implants from computed tomography/magnetic resonance data from a patient. Some advantages of these implants are shorter surgery times, improved biomechanical compatibility, reduction in rejection and infection risks, better ergonomic and esthetic results and increasing the probability of success of the implant [4,6–8]. Recently, Jardini et al. obtained optimal results in surgeries using Ti-6Al-4V customized implants made by DMLS in different cases of large cranial injuries in the right-frontal bone from a bicycle [4] and a motorcycle [5] accidents, and in the left frontoparietal-temporal bone from a cerebrovascular accident [9]. Salmi et al. [8] produced a volumetric net structure for a patient to reconstruct the orbital wall and correct eye asymmetry. Philippe [10] used pure Ti and DMLS in a Le Fort I osteotomy.

However, as DMLS presents high cooling rates, the obtained microstructures and properties are different from commercial materials [11,12]. Mower et al. [13] performed an in-depth study comparing the mechanical behavior of additive manufactured, power-bed laser fused Ti-6Al-4V alloy, with conventional ones. These authors concluded that the α' martensitic microstructure obtained in as-fabricated DMLS Ti-6Al-4V condition shows lower fatigue strength due to a lower ductility and fabrication defects. Therefore, the mechanical properties for as-built Ti-6Al-4V ELI alloy made by DMLS do not achieve the requirements gathered in the ASTM F136 standard for implants [14]. Nevertheless, the application of different post processing treatments enables to match the mechanical properties with the requirements for implant applications [11–13,15].

Similarly, corrosion properties of AM materials also differ from the conventional alloys. Despite this property is crucial for many applications, it has been scarcely studied on these materials [16–18]. Corrosion can be a source of failure of an implant. In addition, ion release by the corrosive attack can cause cytotoxic, genotoxic and immunological effects, either locally or at distance from the implant [19]. Therefore, corrosion resistance of DMLS materials plays a key role for applications in biomedical use. Damborenea et al. [20] observed anomalous behavior of the DMLS Ti-6Al-4V alloy regarding the wrought material. As result of the presence of surface defects, DMLS Ti-6Al-4V alloy showed voluminous corrosion products due to the localized attack developed preferentially on these sites. Therefore, additional protection is required to achieve the same localized corrosion resistance than conventional alloy.

Among different surface modification techniques, the anodizing process can be used to improve corrosion resistance in physiological solutions but also to promote new properties and functionalities into titanium alloys surfaces. Literature has reported that the fluoride content incorporated into the anodic oxide layer from the anodizing bath and their distribution are the responsible for the antibacterial properties as well as improved osteoinductive response [21–25].

Since the anodizing process is dependent on the composition, surface finishing and microstructure of the alloy, the resulting anodic oxide layers after heat treatments may also be different. Thus, the influence of heat treatments on the properties of samples produced by DMLS should be a major objective as happens for the Ti-6Al-4V commercial alloys. In this context, the present study aims to explore the influence of heat treatments in the corrosion behavior of Ti-6Al-4V ELI alloy produced by additive manufacturing as well as their influence on the surface functionalization of this alloy.

2. Material and methods

Cylindrical samples with 10 mm height and 12 mm diameter were produced with Ti-6Al-4V ELI commercial powder from EOS GmbH Electro Optical Systems by a DMLS AM machine EOSINT M270. Processing parameters were a laser power of 170 W, hatch spacing of 100 μm, layer thickness of 30 μm and scanning speed of 1250 mm/s. The laser movement drew a zigzag pattern, turning 45° between layers. An argon shield atmosphere was used as protective gas and for monitoring oxygen level.

All produced samples, except the ones from as-built condition, were stress relieved. The building platform containing the samples was brought to a temperature of 650 °C and maintained for 3 h in vacuum. Subsequently it was furnace cooled. After removing samples from the building platform, three different heat treatments at 850, 950 and 1050 °C were performed in argon atmosphere for one hour and subsequent furnace cooling. The temperatures were chosen considering values below, close and above β transus temperature ($T_\beta = 995$ °C). Table 1 summarizes the conditions evaluated in this work.

The samples for microstructural characterization were mechanically ground, polished and etched with Kroll reagent (5%vol HNO_3, 10%vol HF in H_2O). Micrographs were done by a Zeiss EVO MA15 scanning electron microscope (SEM) and a Leica DM IL LED optical microscope (OM).

Prior to the anodizing process the samples were mechanically ground polished with colloidal silica (0.04 μm), and chemically polished in a solution of HF (40 wt%): HNO_3 (68 wt%): H_2O with volume ratio 1: 4: 5 for 2 min at 20 °C. Finally, the samples were rinsed in distilled water and air dried. Then, anodizing was performed in a two-electrode cell at a constant voltage of 20 V in a 34.5 mM HF and 1 M H_2SO_4 electrolyte at 20 °C for 5 min. A platinum plate was used as cathode.

Roughness (mean and standard deviation in 3 different areas with 8 measurements each) was measured before and after anodizing by a confocal imaging profiler Sensofar Plµ2300. In order to compare the roughness promoted by the anodizing process, all the samples were mechanically polished until an average roughness value, Ra, ~30 nm. Subsequently, they were chemically polished and finally anodized. Roughness measurements were performed after each stage of the anodizing process.

For analyzing the anodic oxide films, a Hitachi S 4800 J (FEG-SEM) equipped with EDS facilities was used. Nanopores diameter was estimated using ImageJ software.

Electrochemical characterization of anodized and non-anodized samples was done by cyclic potentiodynamic polarization curves. Non-anodized samples were tested after chemical polishing. Tests were done in triplicate in a three-electrode cell connected to a Gamry Reference 600 potentiostat. The sample was the working electrode, a Silver–Silver chloride electrode (Ag/AgCl, saturated KCl) the reference electrode and a platinum basket mesh the counter electrode. Electrolyte was a phosphate buffered saline (PBS) solution at 37 ± 2 °C, containing 8.77 g/l of NaCl, 1.36 g/l of KH_2PO_4 and 1.28 g/l of Na_2HPO_4 with pH ranging from 7.2 to 7.3. The sides of the cylindrical samples were masked by an acid resistant lacquer leaving an area of 1 cm^2 exposed to the electrolyte. All the tests were done in aerated conditions. Before electrochemical testing, one-hour period was adopted for open circuit potential stabilization. The curves started from −0.3 V (vs. OCP) to +3 V (vs. Ag/AgCl, saturated KCl), and the reverse scan from +3 V (vs. Ag/AgCl, saturated KCl) to +1.3 V (vs. Ag/AgCl, saturated KCl) at a constant scan rate of 0.16 mV/s. Corrosion current density (A/cm^2) was used to determine the corrosion kinetics of the different samples.

Table 1
Heat treatments conditions for Ti-6Al-4V ELI alloy made by DMLS.

Condition	Temperature (°C)	Time (h)	Heating rate (°C/min)	Cooling
As-built (AB)	—	—	—	—
Stress relieving (SR)	650	3	10	Furnace
HT850	850	1	9.2	Furnace
HT950	950	1	9.2	Furnace
HT1050	1050	1	9.2	Furnace

3. Results and discussion

Fig. 1 shows the optical micrographs -OM-of the grain morphology corresponding to AB, SR, HT850, HT950 and HT1050 conditions. AB (Fig. 1a), SR (Fig. 1b) and HT850 (Fig. 1c) conditions present refined prior β grains resulting from the rapid cooling from β field during the manufacturing process. On the other hand, HT950 condition (Fig. 1d) presents less visible prior β grains with an initial state of new nucleated β grains because the temperature was brought close to T_β. Finally, when temperature was brought above T_β (HT1050 condition), the previous structure is replaced by new β grains. During cooling, lamellar α+β microstructure is formed and prior β grains remain visible (Fig. 1e).

Fig. 2 presents SEM images of the microstructure of the samples after each heat treatment. The as-built condition, AB (Fig. 2a), shows an acicular martensitic structure constituted by α/α' phase platelets. During the manufacturing process, the fast interaction of the laser with the surface melts the material and promotes a rapid cooling from β field, resulting in a martensitic structure. On the other hand, annealed commercial Ti-6Al-4V ELI alloy used in implants typically presents an equiaxial α+β microstructure. As the resulting microstructure from DMLS process is martensitic, heat treatments will have distinct effects compared to commercial alloys [11,12]. Fig. 2b corresponds to the stress relieving condition, SR. Even though the microstructure appears similar to AB condition, at higher magnifications (Fig. 2c) some differences can be observed. For the SR condition the temperature reaches the activation energy for nucleating nanometric β phase (white phase). As the martensitic structure is metastable, stress relieving temperature and applied time (650 °C/3 h) lead to precipitation of small clusters of β phase (aging). β phase was confirmed by the authors in a previous work by means of X-ray diffraction [14]. Fig. 2d and e show the
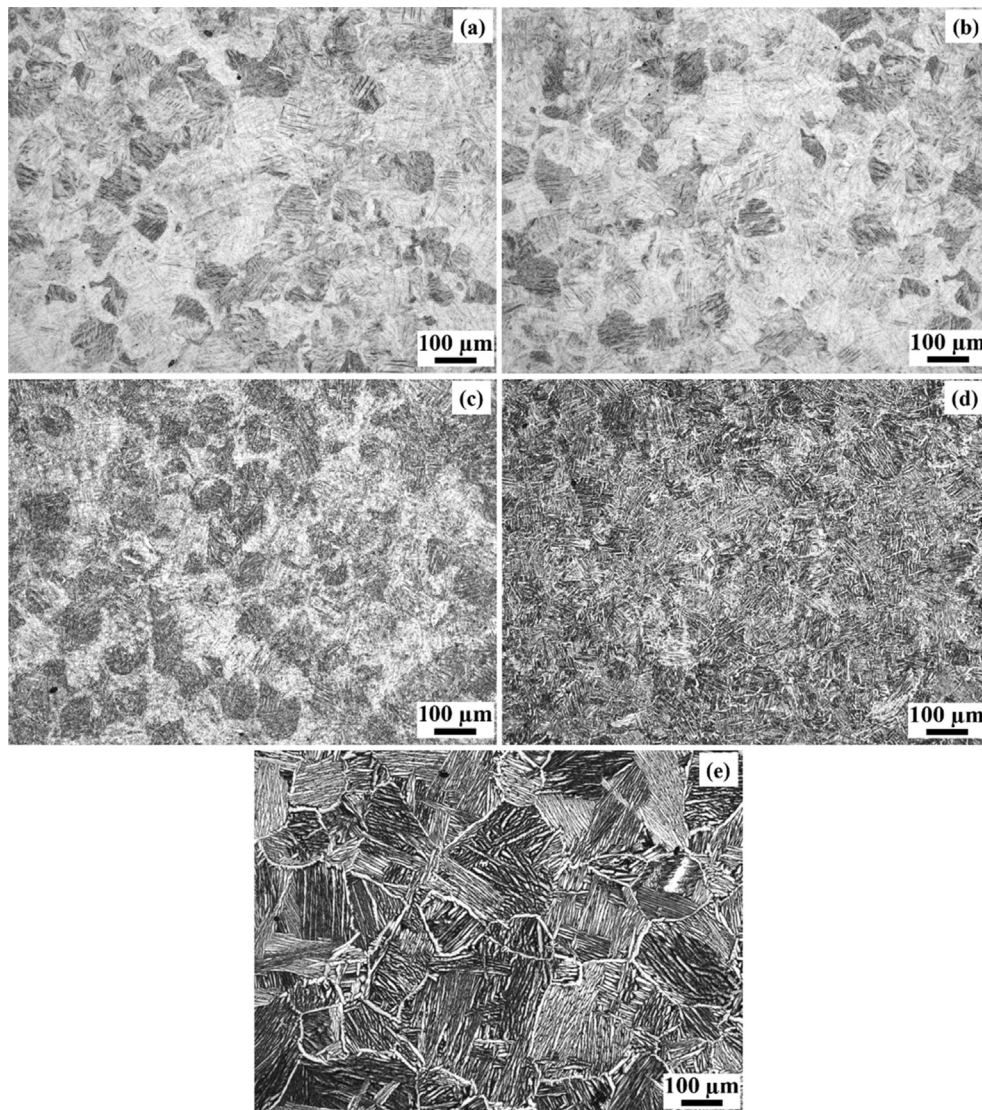

Fig. 1. OM micrographs of heat-treated Ti-6Al-4V ELI alloy made by DMLS. (a) AB, (b) SR, (c) HT850, (d) HT950 and (e) HT1050 conditions.
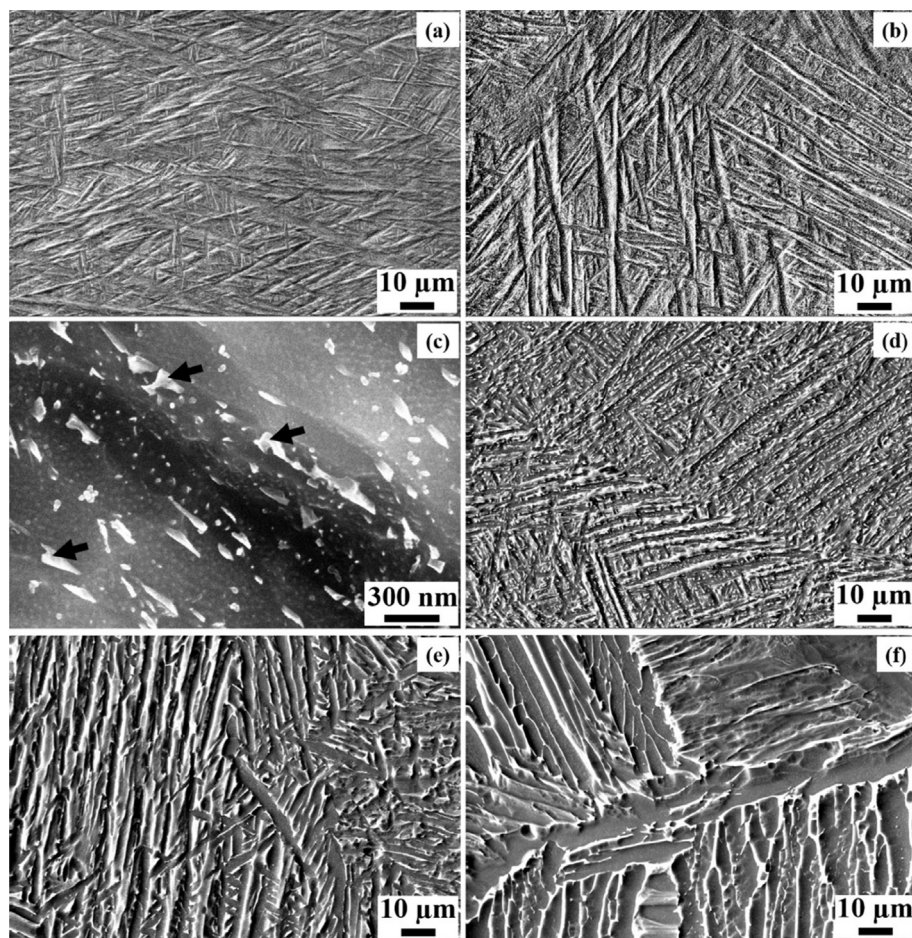
Fig. 2. SEM micrographs of heat-treated Ti-6Al-4V ELI alloy made by DMLS. (a) AB, (b) SR, (c) SR nanometric β phase (indicated by arrows), (d) HT850, (e) HT950 and (f) HT1050 conditions. α phase is dark and β phase is light.

microstructures corresponding to HT850 and HT950 conditions, respectively. In both cases, the microstructure is composed of acicular crystals of α/α' (dark phase) with β crystals (white phase) surrounding the α phase. These heat treatments performed at higher temperatures, which do not exceed $T_β$, transform the α' structure into α phase and, β phase crystals precipitate around α phase by segregation of V through it. In addition, the higher temperature applied for HT950 condition favors growth rather than nucleation, leading to a coarser structure. Finally, for the HT1050 condition, $T_β$ temperature is exceeded and the fully precipitation of β phase is promoted during the heat treatment. As a result, a lamellar α+β microstructure is obtained, as shown in Fig. 2f. Slow cooling rates favor the nucleation of the α phase, which grows preferentially at β phase grain boundaries. After cooling, β phase remains retained between α plates.

As microstructures obtained from DMLS process are different from commercial materials, differences in electrochemical processes, i.e., anodizing and corrosion, may be expected [26–28].

The anodic layer grown on the DMLS Ti-6Al-4V samples have a duplex structure composed by an inner barrier layer and an outer nanoporous layer, as seen in Fig. 3a. The thickness of each layer is similar for all heat treatment conditions; i.e., the barrier layer is ~47 nm, while the thickness of the nanoporous layer is ~38 nm, indicating that the heat treatment has no influence on thickness. The total thickness of the anodic layer is of ~85 nm.

Literature has described the beneficial effects of the incorporation of specific ions, such as F, into the anodic films for enhancing

the antibacterial and osteogenic properties of the alloy [21,23]. In present case, the composition of the film showed that F is incorporated into the anodic layer in a concentration of 5.3 ± 0.2; 5.9 ± 0.8; 5.2 ± 1.0; 5.1 ± 1.0 and 5.8 ± 1.7 (at.%) for AB, SR, HT850, HT950 and HT1050 samples, respectively. Therefore, no matter the heat treatment applied on the alloy, the F content incorporated into de surface ranges about ~5 at.%. The content is in the same order than described in literature for nanoporous anodic films grown on commercial Ti-6Al-4V alloy [23,29,30], ensuring their antibacterial properties.

Although the thickness and F content hardly vary with the heat treatment applied, it does surface morphology. Fig. 3 shows the top view of the anodized heat-treated samples at different conditions. For the AB condition, a homogeneous nanoporous layer, which follows the topography of the material surface, can be seen in Fig. 3b. For the SR condition, the nanoporous surface shows small voids corresponding to the dissolution of the oxide grown on nanometric β phase (Fig. 3c). As the β phase is enriched with vanadium, the anodic layer grown on β phase is enriched in V and has lower stability in the anodizing bath. This results in a higher dissolution of the oxide grown on β phase, leaving cavities over the nanoporous film, as found also in Ti-6Al-4V commercial alloy [31,32]. Nevertheless, after the complete dissolution of the oxide on the β phase, the anodic layer grows on the α'/α matrix placed underneath and a recessed nanoporous layer is observed at the bottom of the former β phase. On the other hand, for HT850, HT950 and HT1050 conditions, shown in Fig. 3d–f, respectively, the β
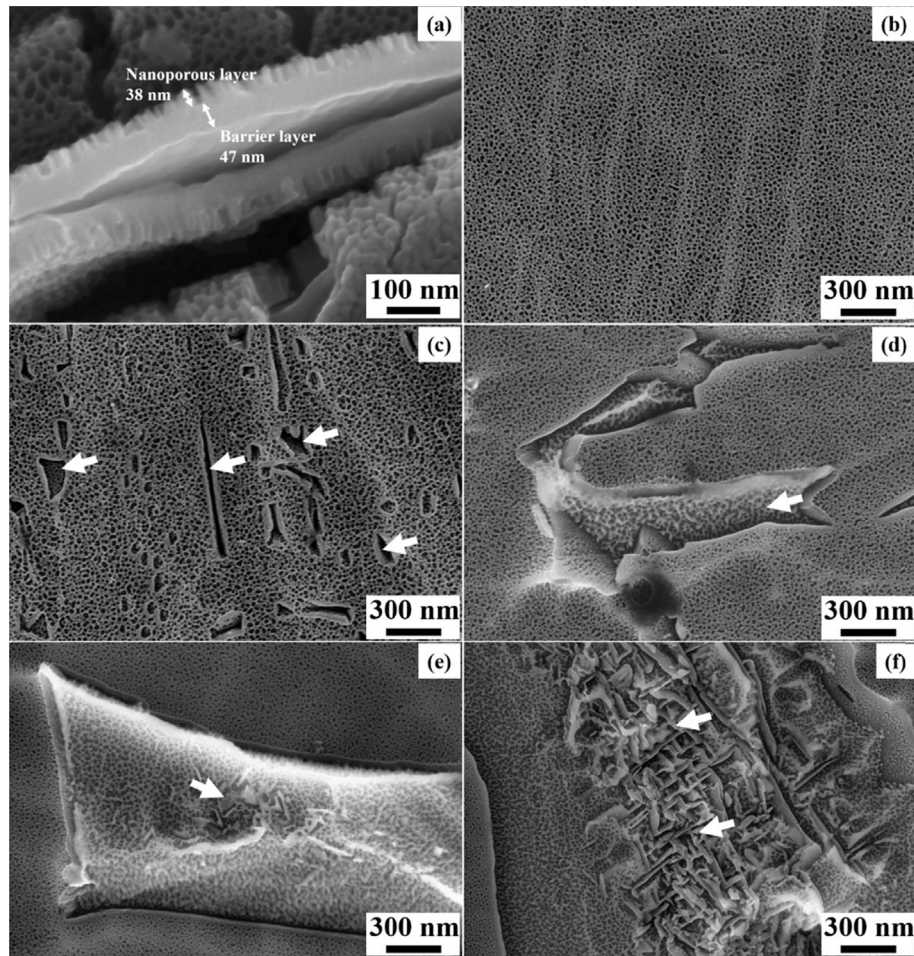
Fig. 3. FEG-SEM micrographs of heat-treated and anodized surfaces of Ti-6Al-4V ELI alloy made by DMLS. (a) Oxide film section view, (b) AB, (c) SR, (d) HT850, (e) HT950 and (f) HT1050 conditions. Arrows in (c) point out voids left by the dissolved β phase. Arrow in (d) indicates nanopores layer grown on β phase. Arrows in (e) and (f) indicate mesoporous structure grown inside β phase.

phase is only partially consumed and it appears covered by a nanoporous layer with a larger pore size [33]. The diameter of the pores on α phase is 14.0 ± 4.7 nm while on β phase is 17.3 ± 6.5 nm. Furthermore, when the size of the β phase reaches a critical size (HT950 and mainly for HT1050 conditions), the order of the nanoporous titanium oxide inside the β phase disappears and presented a mesoporous like structure, as seen in Fig. 3e and f. Literature reports such phenomenon neither on rolled or wrought Ti-6Al-4V alloys nor on AM Ti-6Al-4V alloys. It seems that inside the β phase it might be zones with different composition as in a lamellar structure, so the anodic layer grown might be comprised by zones with less stable oxides and, others with more stable oxides in the anodic bath.

Roughness plays a key role in the development of uniform anodic films. Fig. 4 shows the roughness values measured after each stage of the anodizing process. After chemical polishing, the HT950 and HT1050 samples show higher Ra values in comparison to the AB, SR, and HT850 samples. As chemical polishing is in fact the dissolution of the alloy under controlled conditions, this is strongly dependent on the reactions occurred at the interface of the material surface and the solution, and therefore on the microstructure and grain size [26,34]. Therefore, for the HT950 and HT1050 samples, which show heterogeneous α+β phase microstructure with larger grain size, the roughness and the morphology achieved during the anodizing process is mostly dependent on phase type and size; as

well as grain size. Chemical polishing and anodizing are surface treatments that induce changes in surface roughness. For bio-materials applications the roughness is an important parameter which should be controlled because it conditions the fate of
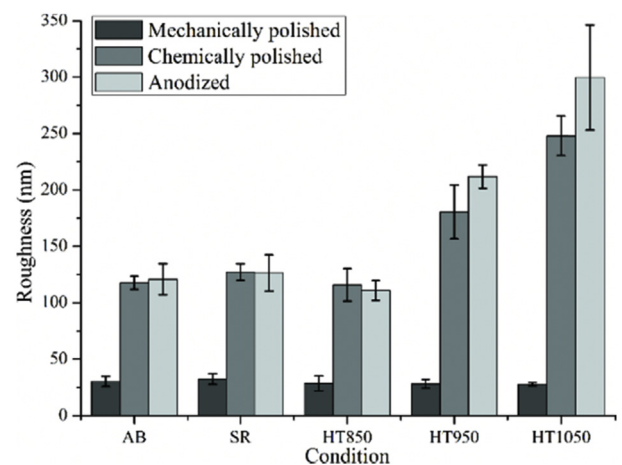

Fig. 4. Roughness measurements after each surface preparation step of heat-treated Ti-6Al-4V ELI alloy made by DMLS.

titanium prosthetic implants. In principle, rough surfaces are beneficial to osseointegration providing mechanical anchorage for hard tissues. However, the greater contact area of rougher surfaces also increases ions release as well as favor bacterial attachment in low blood flow zones [35].

As it is known, microstructure has a major role in corrosion resistance of metallic alloys. However, the AM alloys literature is controversial in this respect. While some authors asses that the martensitic α' structure has lower corrosion resistance, other authors consider this martensitic structure better from corrosion view point, because it is more homogeneous and contains all the alloying elements in solid solution [17,18,28].

Electrochemical studies were performed to evaluate the influence of the bigger size phases, resulting of the heat treatment, on corrosion behavior. Potentiodynamic polarization curves for all samples before and after anodizing process are gathered in Fig. 5. For the non-anodized surfaces, the E_{corr} ranges about -0.20 and -0.27 V (vs. Ag/AgCl, saturated KCl). The anodic branch describes a passive region characterized by a passive current density, i_{pass}, about $0.9 \cdot 10^{-6}$ A/cm^2 which agrees with the values reported

in literature for commercial alloys [27,36]. At approximately 1.3 V (vs. Ag/AgCl, saturated KCl) the curve plots a slight increase in current density associated with changes in the electronic structure of the native oxide film [30,37,38]. However, at higher potential values some differences can be observed depending on the heat treatment. While the AB and SR conditions do not show any pitting potential and the reverse sweep of the anodic branch takes place through lower current densities; the HT850, HT950 and HT1050 conditions presented pitting potential, $E_{pitting}$, at 2.51 V (vs. Ag/AgCl, saturated KCl) and a repassivation potential, E_{repass}, at 1.84 V (vs. Ag/AgCl, saturated KCl). These results suggest that the presence of bigger crystals of β phase in these conditions appears related to a higher susceptibility to localized attack, since the potentiodynamic curves depict pitting potential over 2.5 V (vs. Ag/AgCl, saturated KCl). In contrast, the martensitic microstructure, which has a homogeneous distribution of alloying elements, does not show pitting potential.

These results contrast with those reported by Dai et al. [17,18] when compared the corrosion properties of SLM Ti-6Al-4V and conventional Ti-6Al-4V alloy in NaCl 3.5% and 1 M HCl. They
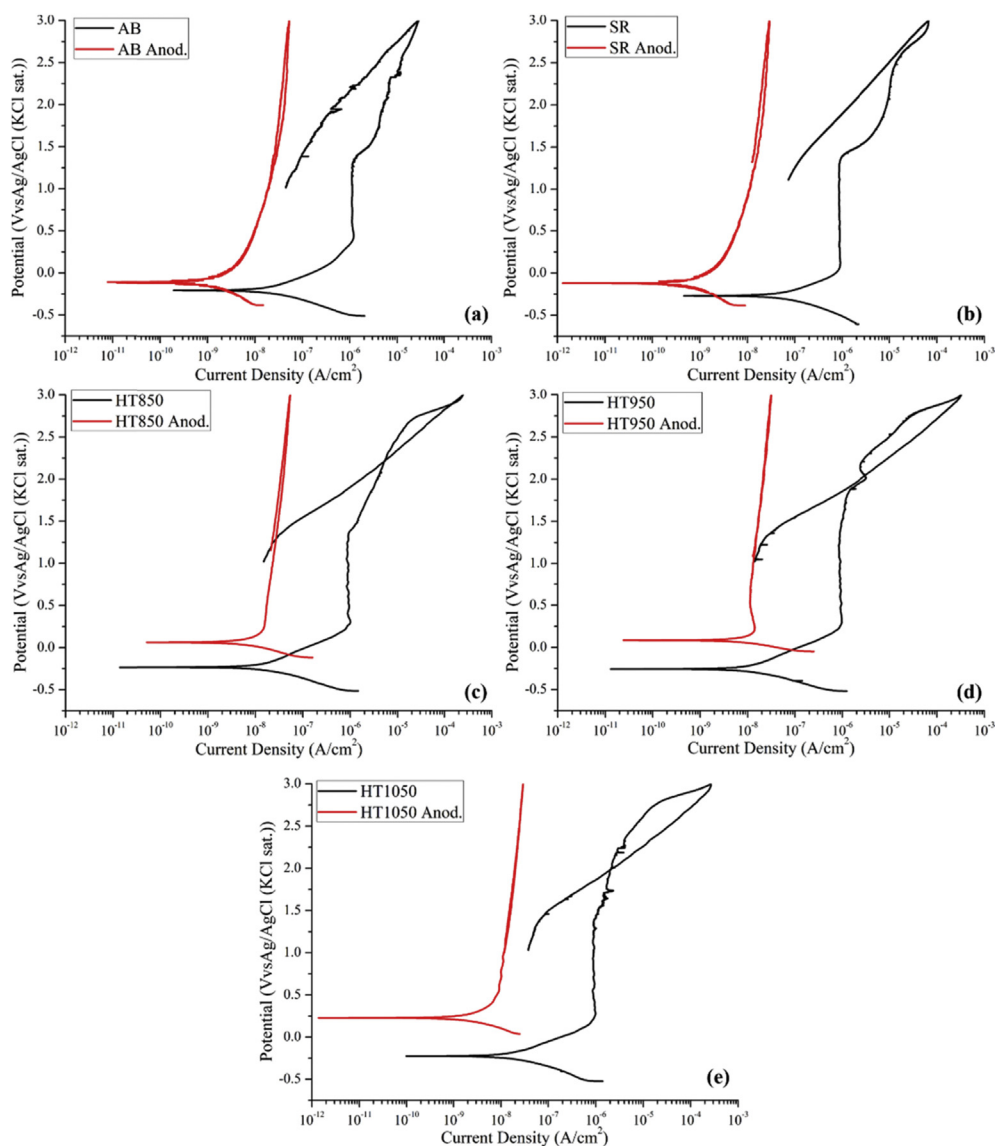

Fig. 5. Cyclic potentiodynamic polarization curves in PBS at 37 °C for different heat treatments of non-anodized and anodized Ti-6Al-4V ELI alloy made by DMLS. (a) AB, (b) SR, (c) HT850, (d) HT950 and (e) HT1050 conditions.

concluded that the lower corrosion resistance obtained for the SLM Ti-6Al-4V is consequence of the higher volume fraction of martensitic α' phase and less content of β phase, in comparison to the $\alpha+\beta$ microstructure of a commercial alloy. According to them, α' is a metastable phase in high energy state more prone to corrosion and, therefore, less resistant from corrosion viewpoint.

Conversely, the results of the present work are consistent with others published in literature. Some authors state that the biphasic microstructure has lower corrosion resistance than fully martensitic, because martensitic α' structure leads to the formation of a more homogeneous native titanium oxide film. Thus, the native oxide grown on $\alpha+\beta$ microstructure is more defective and less homogeneous [28,39]. Vanadium is a β phase stabilizer element, which segregates into β phase during cooling. As the oxide growth on the surface is dependent on the substrate composition, the vanadium enriched oxide formed on β phase has lower stability in chloride containing solutions, so the native oxide film turns more prone to localized attack in such areas, reducing the passivity [27,28]. Moreover, in the biphasic microstructure there are also more interfacial regions, i.e., interfaces between α and β phases, which are more susceptible to corrosion. In this sense Atapour et al. [27] observed that, for $\alpha + \beta$ microstructures, either β phase or interfacial regions are preferential sites for localized attack in 3.5 M HCl solution.

For the anodized samples the E_{corr} values were -0.11, -0.12, 0.06, 0.09 and 0.23 V (vs. Ag/AgCl, saturated KCl) for AB, SR, HT850, HT950 and HT1050 conditions, respectively. The anodic oxide film shows a passive behavior with i_{pass} values about $2-4\cdot10^{-8}$ A/cm^2. These values are two orders of magnitude lower when compared to non-anodized samples. No pitting potential is depicted for any condition and, the reverse anodic branch is fully reversible. This result points out the good barrier properties of the anodic oxide layer grown on the DMLS Ti-6Al-4V alloy for all tested conditions. Regardless the microstructure, the content and size of β phase developed during the heat treatment, the anodizing process enables the growth of a protective oxide layer with improved corrosion resistance to localized attack and lowers corrosion kinetics. Therefore, after the anodizing process the corrosion behavior of the DMLS Ti-6Al-4V alloy is similar to the anodized commercial alloy [36].

These results show that the amorphous oxide layer grown by anodizing [32] blows away the differences in corrosion resistance promoted by the heat treatments applied to improve the mechanical properties of the DMLS Ti-6Al-4V alloy. Thus, the anodizing process applied after the heat treatments allows combining good mechanical properties and corrosion resistance, comparable to the anodized conventional material.

Nevertheless, it is worth noting that the anodizing process must be applied after the heat treatment of the samples. Otherwise, at temperatures near 280 °C the amorphous oxide transforms into anatase, and at temperatures above 650 °C into rutile. Moreover, at such high temperature the nanostructure starts to collapse and the F evaporates, jeopardizing the achieved antibacterial and osteogenic properties too [40].

Finally, the lower corrosion kinetics, regarding the non-anodized samples, implies lower Al and V ions release inside human's body. Consequently, the service life of the implant can be further improved.

4. Conclusions

In this study, samples were produced by DMLS and submitted to different heat treatments to fulfill the mechanical requirements for biomaterial applications. Subsequently, the influence of the microstructures obtained in each case on the anodizing process and on corrosion resistance in PBS solution was evaluated. The obtained microstructures were α/α' phases, acicular crystals of α'/α phases with β phase among the contours and lamellar structure of $\alpha+\beta$ phases. Nucleation and growth of β phase were detrimental to corrosion resistance reducing pitting corrosion resistance on HT850, HT950 and HT1050 samples. Nevertheless, despite the microstructural changes promoted by the heat treatments, the anodic oxide layers reduce passive current density in two orders of magnitude for all the heat treatment conditions and improve pitting corrosion resistance.

Additive manufacturing, combined with heat treatments and anodizing process, can be a powerful tool in development of custom made implants that meet with the mechanical and corrosion requirements. Moreover, the decrease in two orders of magnitude of the corrosion kinetics reduces the risk associated to ion release, which is a key factor in patient's health and in implant durability. Additionally, the incorporation of fluorides into the anodic oxide layer provides supplementary antibacterial and osteogenic properties of interest in biomaterial applications.

In conclusion, this work showed anodizing is a robust technique able to provide corrosion resistance and additional functionalities to DMLS Ti-6Al-4V alloy, comparable to the anodized conventional wrought material.

Acknowledgments

References

[1] R.M. Pilliar, Metallic biomaterials, in: R. Narayan (Ed.), Biomedical Materials, Springer Science + Business Media, LLC, 2009.

[2] C.Y. Guo, J.P. Matinlinna, A.T.H. Tang, Effects of surface charges on dental implants: past, present, and future, Int. J. Biomater. 2012 (2012) 1–5.

[3] G.A. Longhitano, M.A. Larosa, A.L. Jardini, C.A.C. Zavaglia, M.C.F. Ierardi, Surface finishes for Ti-6Al-4V alloy produced by direct metal laser sintering, Mater. Res. 18 (2015) 838–842.

[4] A.L. Jardini, M.A. Larosa, R. Maciel Filho, C.A.C. Zavaglia, L.F. Bernardes, C.S. Lambert, D.R. Calderoni, P. Kharmandayan, Cranial reconstruction: 3D biomodel and custom-built implant created using additive manufacturing, J. Cranio-Maxillo-Fac. Surg. 42 (2014) 1–8.

[5] A.L. Jardini, M.A. Larosa, C.A.C. Zavaglia, L.F. Bernardes, C.S. Lambert, P. Kharmandayan, D.R. Calderoni, R. Maciel Filho, Customised titanium implant fabricated in additive manufacturing for craniomaxillofacial surgery, Virtual Phys. Prototyp. 9 (2014) 115–125.

[6] L.E. Murr, S.A. Quinones, S.M. Gaytan, M.I. Lopez, A. Rodela, E.Y. Martinez, D.H. Hernandez, E. Martinez, F. Medina, R.B. Wicker, Microstructure and mechanical behavior of Ti–6Al–4V produced by rapid-layer manufacturing, for biomedical applications, J. Mech. Behav. Biomed. Mater. 2 (2009) 20–32.

[7] L. Ciocca, M. Fantini, F. Crescenzio, G. Corinaldesi, R. Scotti, Direct metal laser sintering (DMLS) of a customized titanium mesh for prosthetically guided bone regeneration of atrophic maxillary arches, Med. Biol. Eng. Comput. 49 (2011) 1347–1352.

[8] M. Salmi, J. Tuomi, K.S. Paloheimo, R. Björkstrand, M. Paloheimo, J. Salo, R. Kontio, K. Mesimäki, A.A. Mäkitie, Patient-specific reconstruction with 3D modeling and DMLS additive manufacturing, Rapid Prototyp. J. 18 (2012) 209–214.

[9] A.L. Jardini, M.A. Larosa, M.F. Macedo, L.F. Bernardes, C.S. Lambert, C.A.C. Zavaglia, R. Maciel Filho, D.R. Calderoni, E. Ghizoni, P. Kharmandayan, Improvement in cranioplasty: advanced prosthesis biomanufacturing, Proced. CIRP 49 (2016) 203–208.

[10] B. Philippe, Custom-made prefabricated titanium miniplates in Le Fort I osteotomies: principles, procedure and clinical insights, Int. J. Oral Maxillofac. Surg. 42 (2013) 1001–1006.

[11] M. Thöne, S. Leuders, A. Riemer, T. Tröster, H.A. Richard, Influence of heat-treatment on Selective Laser Melting products – e.g. Ti6Al4V, in: Solid Free-form Fabrication Symposium, Austin, Texas, USA, 2012, pp. 492–498.

[12] B. Vrancken, L. Thijs, J.P. Kruth, J. Van Humbeeck, Heat treatment of Ti6Al4V

produced by selective laser melting: microstructure and mechanical properties, J. Alloys Compd. 541 (2012) 177–185.

[13] T.M. Mower, M.J. Long, Mechanical behavior of additive manufactured, powder-bed laser-fused materials, Mater. Sci. Eng., A 651 (2016) 198–213.

[14] G.A. Longhitano, M.A. Larosa, A.L. Jardini, C.A.C. Zavaglia, M.C.F. Ierardi, Correlation between microstructures and mechanical properties under tensile and compression tests of heat-treated Ti-6Al–4V ELI alloy produced by additive manufacturing for biomedical applications, J. Mater. Process. Technol. 252 (2017) 202–210.

[15] Q. Huang, X. Liu, X. Yang, R. Zhang, Z. Shen, Q. Feng, Specific heat treatment of selective laser melted Ti–6Al–4V for biomedical applications, Front. Mater. Sci. 9 (2015) 373–381.

[16] J. Yang, H. Yang, H. Yu, Z. Wang, X. Zeng, Corrosion behaviour of Additive manufactured Ti-6Al-4V alloy in NaCl solution, Metall. Mater. Trans. A 48A (2017) 3583–3593.

[17] N. Dai, L.C. Zhang, J. Zhang, Q. Chen, M. Wu, Corrosion behavior of selective laser melted Ti-6Al-4 V alloy in NaCl solution, Corrosion Sci. 116 (2016), 784-489.

[18] N. Dai, L.C. Zhang, J. Zhang, X. Zhang, Q. Ni, Y. Chen, M. Wu, C. Yang, Distinction in corrosion resistance of selective laser melted Ti-6Al-4Valloy on different planes, Corrosion Sci. 111 (2016) 703–710.

[19] V. Sansone, D. Pagani, M. Melato, The effects on bone cells of metal ions released from orthopaedic implants. A review, Clin. Cases Miner. Bone Metab. 10 (2013) 34–40.

[20] J.J. Damborenea, M.A. Arenas, M.A. Larosa, A.L. Jardini, C.A.C. Zavaglia, A. Conde, Corrosion of Ti6Al4V pins produced by direct metal laser sintering, Appl. Surf. Sci. 393 (2017) 340–347.

[21] K.C. Popat, M. Eltgroth, T.J. LaTempa, C.A. Grimes, T.A. Desai, Staphylococcus epidermis adhesion and increased osteoblast functionality on antibiotic-loaded titania nanotubes, Biomaterials 28 (2007) 4880–4888.

[22] K.C. Popat, L. Leoni, C.A. Grimes, T.A. Desai, Influence of engineered titania nanotubular surfaces on bone cells, Biomaterials 28 (2007) 3188–3197.

[23] C. Pérez-Jorge, A. Conde, M.A. Arenas, R. Pérez-Tanoira, E. Matykina, J.J. Damborenea, E. Gōmez-Barrena, J. Esteban, In vitro assessment of Staphylococcus epidermidis and Staphylococcus aureus adhesion on TiO2 nanotubes on Ti-6Al-4V alloy, J. Biomed. Mater. Res. – part A 100a (2012) 1696–1705.

[24] D. Lozano, J.M. Hernández-López, P. Esbrit, M.A. Arenas, E. Gómez-Barrena, J.J. Damborenea, J. Esteban, C. Pérez-Jorge, R. Pérez-Tanoira, A. Conde, Influence of the nanostructure of F-doped TiO 2 films on osteoblast growth and function, J. Biomed. Mater. Res. – part A 103a (2015) 1985–1990.

[25] M.A. Arenas, C. Pérez-Jorge, A. Conde, E. Matykina, J.M. Hernández-López, R. Pérez-Tanoira, J.J. Damborenea, E. Gómez-Barrena, J. Esteba, Doped TiO2 anodic layers of enhanced antibacterial properties, Colloids Surf., B 105 (2013) 106–112.

[26] X. Liu, P. Chu, C. Ding, Surface modification of titanium, titanium alloys, and related materials for biomedical applications, Mater. Sci. Eng. R Rep. 47 (2004) 49–121.

[27] M. Atapour, A. Pilchak, G.S. Frankel, J.C. Williams, M.H. Fathi, M. Shamanian, Corrosion behavior of Ti-6Al-4V with different thermomechanical treatments and microstructures, Corrosion 66 (2010), 65004-1-65004–9.

[28] I. Cvijović-Alagić, Z. Cvijović, J. Bajat, M. Rakin, Composition and processing effects on the electrochemical characteristics of biomedical titanium alloys, Corrosion Sci. 83 (2014) 245–254.

[29] J.M. Macak, H. Tsuchiya, A. Ghicov, K. Yasuda, R. Hahn, S. Bauer, P. Schmuki, TiO2 nanotubes: self-organized electrochemical formation, properties and applications, Curr. Opin. Solid State Mater. Sci. 11 (2007) 3–18.

[30] J.J. Damborenea, M.A. Larosa, M.A. Arenas, J.M. Hernández-López, A.L. Jardini, M.C.F. Ierardi, C.A.C. Zavaglia, R.M. Filho, A. Conde, Functionalization of Ti6Al4V scaffolds produced by direct metal laser for biomedical applications, Mater. Des. 83 (2015) 6–13.

[31] J.M. Macak, H. Tsuchiya, L. Taveira, A. Ghicov, P. Schmuki, Self-organized nanotubular oxide layers on Ti-6Al-7Nb and Ti-6Al-4V formed by anodization in NH4F solutions, J. Biomed. Mater. Res. - Part A 75 (2005) 928–933.

[32] E. Matykina, J.M. Hernandez-López, A. Conde, C. Domingo, J.J. Damborenea, M.A. Arenas, Morphologies of nanostructured TiO2 doped with F on Ti–6Al–4V alloy, Electrochim. Acta 56 (2011) 2221–2229.

[33] E. Matykina, A. Conde, J. Damborenea, D. Martín y Marero, M.A. Arenas, Growth of TiO2-based nanotubes on Ti–6Al–4V alloy, Electrochim. Acta 56 (2011) 9209–9218.

[34] J. Lausmaa, Mechanical, thermal, chemical and electrochemical surface treatment of titanium, in: D.M. Brunette, P. Tengvall, M. Textor, P. Thomsen (Eds.), Titanium in Medicine, Springer-Verlag Berlin Heidelberg, 2001, pp. 232–258.

[35] G.A. Longhitano, M.A. Larosa, A.L.J. Munhoz, C.A.C. Zavaglia, M.C.F. Ierardi, Surface finishes for Ti-6Al-4V alloy produced by direct metal laser sintering, Mat. Res. 18 (2015) 838–842.

[36] J.M. Hernández-López, A. Conde, J.J. Damborenea, M.A. Arenas, Electrochemical response of TiO2 anodic layers fabricated on Ti6Al4V alloy with nanoporous, dual and nanotubular morphology, Corrosion Sci. 112 (2016) 194–203.

[37] V.A. Alves, R.Q. Reis, I.C.B. Santos, D.G. Souza, T.F. Gonçalves, M.A. Pereira-da-Silva, A. Rossi, L.A. da Silva, In situ impedance spectroscopy study of the electrochemical corrosion of Ti and Ti-6Al-4V in simulated body fluid at 25 °C and 37 °C, Corrosion Sci. 51 (2009) 2473–2482.

[38] P. Acevedo-Peña, G. Vázquez, D. Laverde, J.E. Pedraza-Rosas, I. González, Influence of structural transformations over the electrochemical behavior of Ti anodic films grown in 0.1 M NaOH, J. Solid State Electrochem. 14 (2010) 757–767.

[39] I. Cvijović-Alagić, Z. Cvijović, S. Mitrović, V. Panić, M. Rakin, Wear and corrosion behaviour of Ti-13Nb-13Zr and Ti-6Al-4V alloys in simulated physiological solution, Corrosion Sci. 53 (2011) 796–808.

[40] P. Schmuki, P. Roy, S. Berger, TiO2 nanotubes: synthesis and applications, Angew. Chem. Int. Ed. 50 (2011) 2904–2939.